

# First principles study of thermal conductivity of $\text{In}_2\text{O}_3$ in relation to $\text{Al}_2\text{O}_3$ , $\text{Ga}_2\text{O}_3$ , and $\text{KTaO}_3$

Alaska Subedi

CPHT, CNRS, Ecole Polytechnique, IP Paris, F-91128 Palaiseau, France and  
Collège de France, 11 place Marcelin Berthelot, 75005 Paris, France

(Dated: January 8, 2021)

I use first principles calculations to investigate the thermal conductivity of  $\beta\text{-In}_2\text{O}_3$  and compare the results with that of  $\alpha\text{-Al}_2\text{O}_3$ ,  $\beta\text{-Ga}_2\text{O}_3$ , and  $\text{KTaO}_3$ . The calculated thermal conductivity of  $\beta\text{-In}_2\text{O}_3$  agrees well with the experimental data obtain recently, which found that the low-temperature thermal conductivity in this material can reach values above 1000 W/mK. I find that the calculated thermal conductivity of  $\beta\text{-Ga}_2\text{O}_3$  is larger than that of  $\beta\text{-In}_2\text{O}_3$  at all temperatures, which implies that  $\beta\text{-Ga}_2\text{O}_3$  should also exhibit high values of thermal conductivity at low temperatures. The thermal conductivity of  $\text{KTaO}_3$  calculated ignoring the temperature-dependent phonon softening of low-frequency modes give high-temperature values similar that of  $\beta\text{-Ga}_2\text{O}_3$ . However, the calculated thermal conductivity of  $\text{KTaO}_3$  does not increase as steeply as that of the binary compounds at low temperatures, which results in  $\text{KTaO}_3$  having the lowest low-temperature thermal conductivity despite having acoustic phonon velocities larger than that of  $\beta\text{-Ga}_2\text{O}_3$  and  $\beta\text{-In}_2\text{O}_3$ . I attribute this to the fact that the acoustic phonon velocities at low frequencies in  $\text{KTaO}_3$  is less uniformly distributed because its acoustic phonon branches are more dispersive compared to the binary oxides, which causes enhanced momentum loss even during the normal phonon-phonon scattering processes. I also calculate thermal diffusivity using the theoretically obtained thermal conductivity and heat capacit and find that all four materials exhibit the expected  $T^{-1}$  behavior at high temperatures. Additionally, the calculated ratio of the average phonon scattering time to Planckian time is larger than the lower bound of 1 that has been observed empirically in numerous other materials.

## INTRODUCTION

$\beta\text{-In}_2\text{O}_3$  is a technologically important material due to its use as a transparent conductor when doped with tin [1, 2]. In addition, it has been viewed as a potential candidate for use in high-power devices along with other binary oxides  $\alpha\text{-Al}_2\text{O}_3$  and  $\beta\text{-Ga}_2\text{O}_3$  from the same column of the periodic table because of its wide band gap. A limiting factor in high-power applications is the ability to dissipate heat that is generated in the devices. The thermal conductivity of single-crystal  $\alpha\text{-Al}_2\text{O}_3$  and  $\beta\text{-Ga}_2\text{O}_3$  have been studied both experimentally and theoretically [3–13], which show that these materials are worse conductors of heat than silicon with the room-temperature (300 K) values of  $\sim 35$ ,  $\sim 20$  and  $\sim 150$  W/mK [14], respectively.

In contrast, thermal properties of single-crystal  $\beta\text{-In}_2\text{O}_3$  have received relatively little attention due to difficulty in growing them. Recently, Galazka *et al.* have developed a method to grow  $\text{cm}^3$  size single crystals of  $\beta\text{-In}_2\text{O}_3$  [15, 16], and their thermal conductivity from 20 to 300 K has been measured by Xu *et al.* [17]. They find room-temperature (300 K) thermal conductivity of 15 W/mK, which is slightly worse than that of  $\alpha\text{-Al}_2\text{O}_3$  and  $\beta\text{-Ga}_2\text{O}_3$ . Surprisingly, they also find that the thermal conductivity of  $\beta\text{-In}_2\text{O}_3$  increases rapidly as the temperature is lowered, with a peak value as high as 5000 W/mK at 20 K that is surpassed by few other insulators such as  $\alpha\text{-Al}_2\text{O}_3$  [3] and diamond [18]. Remarkably, experiments on  $\beta\text{-Ga}_2\text{O}_3$  show a peak thermal conductivity of only 530 W/mK at 25 K [8]. These results motive a theoreti-

cal investigation of the thermal conductivity of  $\beta\text{-In}_2\text{O}_3$  so that a comparative study of the microscopic mechanism of thermal transport in these binary oxides can be performed.

Behnia, who was part of the group that measured the thermal conductivity of  $\beta\text{-In}_2\text{O}_3$  [17], asked me: i) why the thermal conductivity of  $\beta\text{-In}_2\text{O}_3$  peaks at such a high value, and ii) why ternary oxides do not show similar high peaks at low temperatures. In this paper, I attempt to answer his questions using first principles calculations of phonon dispersions and three-phonon scattering interactions, which I incorporate in the solution of the Boltzmann transport equation (BTE) to obtain the lattice thermal conductivity. In addition to the binary oxides  $\alpha\text{-Al}_2\text{O}_3$ ,  $\beta\text{-Ga}_2\text{O}_3$  and  $\beta\text{-In}_2\text{O}_3$ , I also study the simplest ternary oxide  $\text{KTaO}_3$  without incorporating its phonon softening effects to investigate the consequence of having an extra atomic species on the low-temperature thermal conductivity. I find the thermal conductivity of  $\beta\text{-In}_2\text{O}_3$  at 300 K is 10 W/mK, and it increases to  $1.2 \times 10^3$  W/mK at 30 K (the lowest temperature that I could solve the BTE). These calculated values are lower than the measured value of 15 W/mK [17], but they capture the three orders of magnitude increase in thermal conductivity as the temperature is lowered. I find that the thermal conductivity of ternary  $\text{KTaO}_3$  rises more slowly than the binary oxides. I attribute this to the fact that velocities of the acoustic phonon branches are distributed more evenly in the binary oxides compared to the ternary  $\text{KTaO}_3$ , which should cause relatively less loss in momentum during the three-phonon scattering processes in the

binary oxides relative to  $\text{KTaO}_3$ .

## CRYSTAL STRUCTURES AND COMPUTATIONAL APPROACH

The three binary  $X_2\text{O}_3$  ( $X = \text{Al}$ ,  $\text{Ga}$  and  $\text{In}$ ) compounds and the ternary  $\text{KTaO}_3$  all occur with different crystal structures, which are shown in Fig. 1.  $\alpha\text{-Al}_2\text{O}_3$  has a layered trigonal structure with the space group  $R\bar{3}c$  containing 10 atoms in the primitive unit cell. Each layer consists of edge-shared  $\text{AlO}_6$  octahedra arranged in a honeycomb pattern, and the layers are stacked such that each octahedron shares edges with the layers above and below it.  $\beta\text{-Ga}_2\text{O}_3$  has a highly anisotropic monoclinic structure with the space group  $C2/m$ , and its primitive unit cell also contains 10 atoms. There are two nonequivalent Ga sites with tetrahedral and octahedral oxygen coordinations, respectively. The  $\text{GaO}_4$  tetrahedra share their corners with  $\text{GaO}_6$  octahedra, and each  $\text{GaO}_6$  octahedron additionally has four edge-shared  $\text{GaO}_6$  octahedra as neighbors.  $\beta\text{-In}_2\text{O}_3$  occurs in the cubic bixbyite structure with the space group  $Ia\bar{3}$  and has 40 atoms in its primitive unit cell. The structure consists of two inequivalent  $\text{InO}_6$  octahedra, one undistorted and another highly distorted, and each of them has six edge-shared and six corner-shared neighbors.  $\text{KTaO}_3$  has the simplest structure among all four compounds being studied in this work, occurring in cubic perovskite structure with the space group  $Pm\bar{3}m$ . Its primitive unit cell has five atoms, with the Ta ions situated inside corner-shared oxygen octahedra.

I calculated the second- and third-order interatomic force constants (IFCs) of these four materials from first principles using density functional theory. These were used to construct the linearized BTE

$$\mathbf{F}_\lambda = \tau_\lambda(\mathbf{v}_\tau + \mathbf{\Delta}_\lambda), \quad (1)$$

where  $\tau_\lambda$  is the relaxation time of the phonon mode  $\lambda$  obtained using perturbation theory,  $\mathbf{v}_\tau$  is the mode's group velocity, and  $\mathbf{\Delta}_\lambda$  is the correction to the population of the mode  $\lambda$  obtained from the simple relaxation time approach. Eq. 1 was solved iteratively using the SHENGBTE package [19] to obtain the lattice thermal conductivity tensor  $\kappa^{\alpha\beta}$ , which is given by the expression

$$\kappa^{\alpha\beta} = \sum_{\lambda} C_{\lambda} v_{\lambda}^{\alpha} F_{\lambda}^{\beta}. \quad (2)$$

Here,  $C_{\lambda}$  is the contribution of mode  $\lambda$  to the specific heat. In addition to the  $\kappa^{\alpha\beta}$ , SHENGBTE was also used to compute group velocities and Grüneisen parameter  $\gamma$  [21] of each phonon mode, phonon contribution to heat capacity per mole  $C$ , and the weighted three-phonon scattering phase space  $W$  [20].

The density functional calculations were performed using the plane-wave projector-augmented-wave method

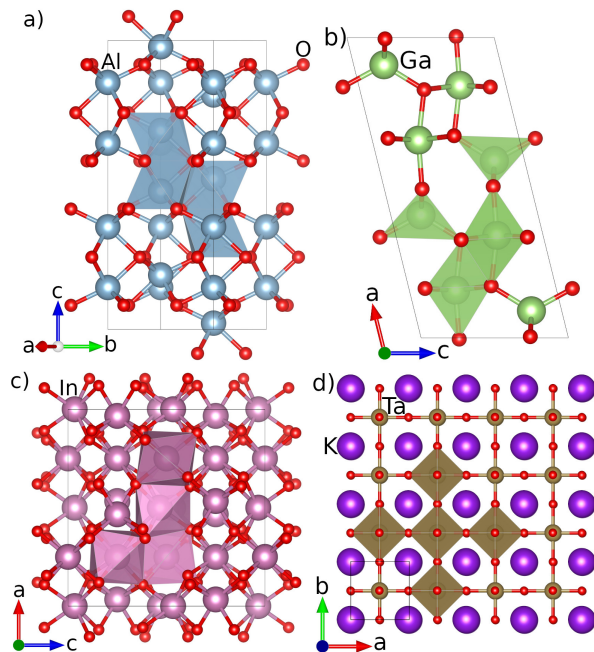


FIG. 1. Crystal structures of a)  $\alpha\text{-Al}_2\text{O}_3$ , b)  $\beta\text{-Ga}_2\text{O}_3$ , c)  $\beta\text{-In}_2\text{O}_3$ , and d) cubic  $\text{KTaO}_3$ . Some polyhedra are drawn to illustrate how they are connected to each other.

within the local density approximation (LDA), as implemented in the VASP software package [22]. A plane-wave cutoff of 520 eV for basis set expansion was used in all calculations. I used potentials in which the  $3s$  and  $3p$  (Al),  $3d$ ,  $4s$ , and  $4p$  (Ga),  $4d$ ,  $5s$ , and  $5p$  (In), and  $2s$  and  $2p$  (O) were treated explicitly as valence electrons. The interatomic potentials were obtained using fully relaxed structures minimizing both the stresses and forces. The Brillouin zone integration in the structural relaxation calculations were performed via  $k$ -point meshes of  $9 \times 9 \times 9$  ( $\alpha\text{-Al}_2\text{O}_3$ ),  $12 \times 12 \times 6$  ( $\beta\text{-Ga}_2\text{O}_3$ ),  $4 \times 4 \times 4$  ( $\beta\text{-In}_2\text{O}_3$ ), and  $12 \times 12 \times 12$  ( $\text{KTaO}_3$ ). The fully-relaxed lattice parameters are  $a = 5.096 \text{ \AA}$  and  $\alpha = 55.36^\circ$  ( $\alpha\text{-Al}_2\text{O}_3$ ),  $a = 12.160$ ,  $b = 3.025$ ,  $c = 5.768 \text{ \AA}$ , and  $\beta = 103.75^\circ$  ( $\beta\text{-Ga}_2\text{O}_3$ ),  $a = 10.705 \text{ \AA}$  ( $\beta\text{-In}_2\text{O}_3$ ), and  $a = 3.960 \text{ \AA}$  ( $\text{KTaO}_3$ ). For  $\beta\text{-Ga}_2\text{O}_3$ , there is an ambiguity in the choice of primitive cell lattice parameters and the Brillouin zone. I chose the convention used in Ref. [23].

The harmonic second-order IFCs and phonon dispersions were obtained using the real-space supercell-based frozen phonon method, as implemented in the PHONOPY package [24]. The third-order IFCs were also obtained using the real-space supercell approach, as implemented in the THIRDORDER.PY program of the SHENGBTE package. The supercells and  $k$ -point meshes used in the calculations of the IFCs, as well as the phonon momentum-space  $q$ -point meshes used in the solution of the Boltzmann transport equation for the four compounds are given in Table I.

TABLE I. Dimensions of the supercells and  $k$ -meshes used in the calculations of second- and third-order IFCs, as well as that of the momentum-space  $q$ -mesh used in the solution of the BTE for all four compounds studied in this work.

	second-order IFCs		third-order IFCs		BTE
	supercell	$k$ -mesh	supercell	$k$ -mesh	$q$ -mesh
$\alpha$ -Al <sub>2</sub> O <sub>3</sub>	4×4×4	3×3×3	3×3×3	3×3×3	14×14×14
$\beta$ -Ga <sub>2</sub> O <sub>3</sub>	4×4×4	3×3×2	3×3×3	3×3×2	12×14×12
$\beta$ -In <sub>2</sub> O <sub>3</sub>	2×2×2	2×2×2	2×2×2	2×2×2	9×9×9
KTaO <sub>3</sub>	4×4×4	3×3×3	4×4×4	4×4×4	18×18×18

## RESULTS AND DISCUSSION

The calculated effective thermal conductivities ( $\kappa = \text{Tr}(\kappa^{\alpha\beta})/3$ ) of  $\alpha$ -Al<sub>2</sub>O<sub>3</sub>,  $\beta$ -Ga<sub>2</sub>O<sub>3</sub>,  $\beta$ -In<sub>2</sub>O<sub>3</sub>, and KTaO<sub>3</sub> using the fully relaxed LDA structures are shown in Fig. 1 along with the respective experimental data. Additionally, the calculated and experimental values at 100 and 300 K are given in Table II. My calculated thermal conductivity for  $\alpha$ -Al<sub>2</sub>O<sub>3</sub> is in excellent agreement with a previous theoretical study [5]. The calculated and experimental [4]  $\kappa$  for  $\alpha$ -Al<sub>2</sub>O<sub>3</sub> agree very well at 300 K, but the experimental  $\kappa$  at 100 K is larger than the calculated value by 22%.

There are three previous calculations of  $\beta$ -Ga<sub>2</sub>O<sub>3</sub>'s [11–13]. My results agree more with that of Ref. [11] than the other two, presumably because we both use LDA while the other two studies use the generalized gradient approximation. The calculated  $\kappa$  from the present study shows excellent agreement at 100 K compared to the experimental data from Ref. [7], but it overestimates the experimental value at 300 K by 30%.

For  $\beta$ -In<sub>2</sub>O<sub>3</sub>, the experimental  $\kappa$  from Xu *et al.* [17] for their most conductive sample that was annealed in the presence of H<sub>2</sub> (shown in Fig. 2) is systematically larger than the calculated one from the present study at every temperature. They find that the thermal conductivity of samples annealed in O<sub>2</sub>, and additionally in H<sub>2</sub>, peaks to values above a thousand W/mK at temperatures below 30 K, but as-grown and air-annealed samples show peaks that reach only up to 500 W/mK. My results show that the intrinsic  $\kappa$  of  $\beta$ -In<sub>2</sub>O<sub>3</sub> reaches as high as 1200 W/mK at 30 K, which indicates that the high thermal conductivity in  $\beta$ -In<sub>2</sub>O<sub>3</sub> measured in Ref. [17] reflects the intrinsic transport property of the material. Nevertheless, the fact that my calculations underestimate the experimental  $\kappa$  suggests that impurities may still play a role in enhancing the thermal conductivity of this material. Anyway, the experimental thermal conductivity of all samples start to converge above 100 K. The experimental  $\kappa$  at 100 and 300 K of  $\beta$ -In<sub>2</sub>O<sub>3</sub> annealed in O<sub>2</sub> is given in Table II, and they are larger than the theoretical values by around 33%. Interestingly, my calculations show that the effective thermal conductivity of  $\beta$ -Ga<sub>2</sub>O<sub>3</sub>

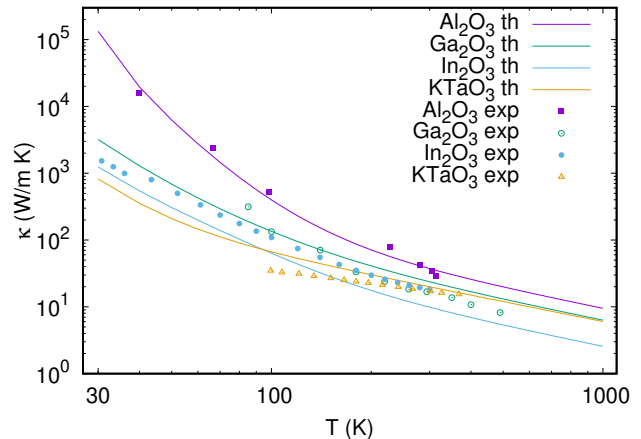


FIG. 2. Calculated effective thermal conductivity ( $\kappa = \text{Tr}(\kappa^{\alpha\beta})/3$ ) of  $\alpha$ -Al<sub>2</sub>O<sub>3</sub>,  $\beta$ -Ga<sub>2</sub>O<sub>3</sub>,  $\beta$ -In<sub>2</sub>O<sub>3</sub>, and KTaO<sub>3</sub> using the fully relaxed LDA crystal structures (solid lines). The experimental values are extracted from Refs. [4, 7, 17, 28] for  $\alpha$ -Al<sub>2</sub>O<sub>3</sub>,  $\beta$ -Ga<sub>2</sub>O<sub>3</sub>,  $\beta$ -In<sub>2</sub>O<sub>3</sub>, and KTaO<sub>3</sub>, respectively.

TABLE II. Calculated and experimental effective thermal conductivity ( $\kappa = \text{Tr}(\kappa^{\alpha\beta})/3$ ) of  $\alpha$ -Al<sub>2</sub>O<sub>3</sub>,  $\beta$ -Ga<sub>2</sub>O<sub>3</sub>,  $\beta$ -In<sub>2</sub>O<sub>3</sub>, and KTaO<sub>3</sub> at 100 and 300 K. The experimental values are extracted from Refs. [4, 7, 17, 28]. The values are given in the units of W/mK.

	100 K		300 K	
	$\kappa^{\text{th}}$	$\kappa^{\text{exp}}$	$\kappa^{\text{th}}$	$\kappa^{\text{exp}}$
$\alpha$ -Al <sub>2</sub> O <sub>3</sub>	399.19	516	37.38	34
$\beta$ -Ga <sub>2</sub> O <sub>3</sub>	134.91	133	23.75	17
$\beta$ -In <sub>2</sub> O <sub>3</sub>	63.52	95	9.88	15
KTaO <sub>3</sub>	66.60	35	19.95	17

is larger than that of  $\beta$ -In<sub>2</sub>O<sub>3</sub> at every temperature. This implies that  $\beta$ -Ga<sub>2</sub>O<sub>3</sub> may show peak thermal conductivity of at least a thousand W/mK at low temperatures.

Lastly, the calculated  $\kappa$  of KTaO<sub>3</sub> is in good agreement with the experimental values [28] above 300 K. At lower temperatures, the theoretical values greatly overestimate the experiment, which is likely due to the neglect of temperature dependent phonon softening of low frequency phonons that is experimentally observed in the material. A similar approximation in the calculation of thermal conductivity of this material was made in a previous theoretical study [25], whose results are well reproduced here. The disregard for phonon softening effects means that the calculations does not explain the low-temperature thermal conductivity of KTaO<sub>3</sub>. Nevertheless, these calculations are helpful in illustrating the differences in the mechanism for thermal transport between the binary and ternary oxides.

Even though the three binary compounds occur in structures with different cation-oxygen bonding environment and network, they follow a decreasing trend in the magnitude of thermal conductivity as the atomic mass

of their cation increases. This is consistent with the conventional wisdom that low atomic mass is conducive to high thermal conductivity [26]. But a comparison with  $\text{KTaO}_3$ , which has a relatively simple cubic perovskite structure, shows that interatomic properties can play an even larger role in determining the thermal conductivity. The average atomic masses of the cations in  $\text{In}_2\text{O}_3$  and  $\text{KTaO}_3$  differ by only 4%, but the calculated thermal conductivity at 400 K of  $\text{KTaO}_3$  is closer to that of  $\text{Ga}_2\text{O}_3$ , whose cation atomic weight is lower by 37%. Therefore, it is instructive to examine the microscopic interatomic quantities to identify the main factors influencing the thermal conductivity of a material.

The calculated phonon dispersions of all four materials being studied in this work are shown in the left column of Fig. 3, and the respective phonon density of states (PHDOS) are shown in Fig. 4.  $\text{KTaO}_3$  has the most uncluttered phonon dispersions, reflecting its simple perovskite structure with only five atoms per primitive unit cell. The intricacy of the dispersions increases as the complexity of the crystal structure increases from  $\alpha\text{-Al}_2\text{O}_3$  to  $\beta\text{-Ga}_2\text{O}_3$  to  $\beta\text{-In}_2\text{O}_3$ . It has been previously noted that complex crystal structures and phonon dispersions both lead to low values of thermal conductivity at high temperatures [26, 27]. Indeed, these four compounds have five or more atoms per unit cell, and their calculated thermal conductivity decrease strongly at high temperatures, becoming less than 10 W/mK at 1000 K. Nevertheless, the thermal conductivity at 1000 K of  $\text{KTaO}_3$  (6 W/mK) is appreciably smaller than that of  $\text{Al}_2\text{O}_3$  (9.3 W/mK), which shows that having a more complex and dense phonon dispersions at high frequencies does not necessarily lead to lower thermal conductivity at high temperatures.

Since lattice thermal conductivity is proportional to the square of the group velocities of phonons, high acoustic phonon velocities should lead to large values of thermal conductivity, especially at low temperatures where heat is mostly carried by long-wavelength acoustic phonons. The right column of Fig. 3 shows the norm of the velocity of each phonon mode as a function of frequency in the four materials.  $\alpha\text{-Al}_2\text{O}_3$  has the highest value of thermal conductivity, and its acoustic phonons indeed have the highest velocities that reach up to 11.3 km/s. However,  $\text{KTaO}_3$  and  $\beta\text{-Ga}_2\text{O}_3$  have similarly high values of acoustic phonon velocities, but the calculated thermal conductivity of  $\text{KTaO}_3$  is almost four times lower than that of  $\beta\text{-Ga}_2\text{O}_3$  in the low-temperature limit. In fact, the acoustic phonon velocities of  $\text{KTaO}_3$  are higher than that of  $\beta\text{-In}_2\text{O}_3$ , but the low-temperature thermal conductivity of  $\text{KTaO}_3$  is lower. This suggests that merely having high acoustic phonon velocities does not necessarily imply high thermal conductivity in the low temperature regime.

A closer look at Fig. 3 shows that the phonon velocity distributions at low frequencies in the binary com-

pounds are less dispersive than in  $\text{KTaO}_3$ . In  $\alpha\text{-Al}_2\text{O}_3$  and  $\beta\text{-In}_2\text{O}_3$ , the acoustic phonon velocities are bunched up in two narrow groups deriving from the respective transverse and longitudinal branches for phonons with frequencies less than  $50\text{ cm}^{-1}$ . The acoustic phonon velocity distribution is slightly wider in  $\beta\text{-Ga}_2\text{O}_3$ , but the velocities still do not get lower than 2.2 km/s for the acoustic phonons below  $50\text{ cm}^{-1}$  in frequency. In contrast, the low-frequency velocity distribution in the same frequency window is more scattered in  $\text{KTaO}_3$ , and the phonon velocities get as low as 1.4 km/s. When acoustic phonons at low frequencies occur with a wide range of velocities, the loss of momentum when they collide with each other during heat transport is more enhanced even for normal scattering processes. Therefore, a more uniform distribution of phonon velocities with smaller magnitudes is likely to yield higher thermal conductivity than a phonon velocity distribution with high velocities that rapidly change as a function of frequency.

The phonon velocity distribution shown in Fig. 3(right) can also qualitatively account for why the high-temperature thermal conductivities of  $\alpha\text{-Al}_2\text{O}_3$ ,  $\beta\text{-Ga}_2\text{O}_3$  and  $\text{KTaO}_3$  are larger than that of  $\beta\text{-In}_2\text{O}_3$ . The optical phonon branches of  $\beta\text{-In}_2\text{O}_3$  only extend up to  $625\text{ cm}^{-1}$ , and they have comparatively small magnitudes of velocities with values less than 2.8 km/s. In contrast, the optical branches of  $\alpha\text{-Al}_2\text{O}_3$ ,  $\beta\text{-Ga}_2\text{O}_3$  and  $\text{KTaO}_3$  extend up to at least  $800\text{ cm}^{-1}$ , and some of these high-frequency optical phonons have velocity in excess of 4 km/s. Therefore, the differences in the phonon velocities of the high-frequency optical phonons of these materials partially explains the differences in their high-temperature thermal conductivity.

Other microscopic quantities such as PHDOS, heat capacity, three-phonon scattering phase space and Grüneisen parameter also play a role in determining the lattice thermal conductivity of a material, but their relative influence have been debated. As one can see in Fig. 4, it is difficult to gain much understanding of the difference in the calculated thermal conductivities of the four compounds by analyzing their phonon density of states. Both  $\beta\text{-Ga}_2\text{O}_3$  and  $\text{KTaO}_3$  have similar values of PHDOS up to  $40\text{ cm}^{-1}$ , but their low-temperature thermal conductivities differ by more than a factor of two. Above  $300\text{ cm}^{-1}$ , the PHDOS of the four compounds overlap considerably, and there is no obvious structure in the PHDOS to account for the different values of the calculated thermal conductivities of the four materials at high temperatures. Similarly, the differences in the calculated lattice heat capacity of the four materials shown in Fig. 5 also does not qualitatively account for the variance in the thermal conductivity at any given temperatures. For example,  $\alpha\text{-Al}_2\text{O}_3$  has the highest calculated thermal conductivity among the four compounds at all temperatures, but it has the lowest heat capacity and reaches saturation less rapidly reflecting its slowly increasing PHDOS.

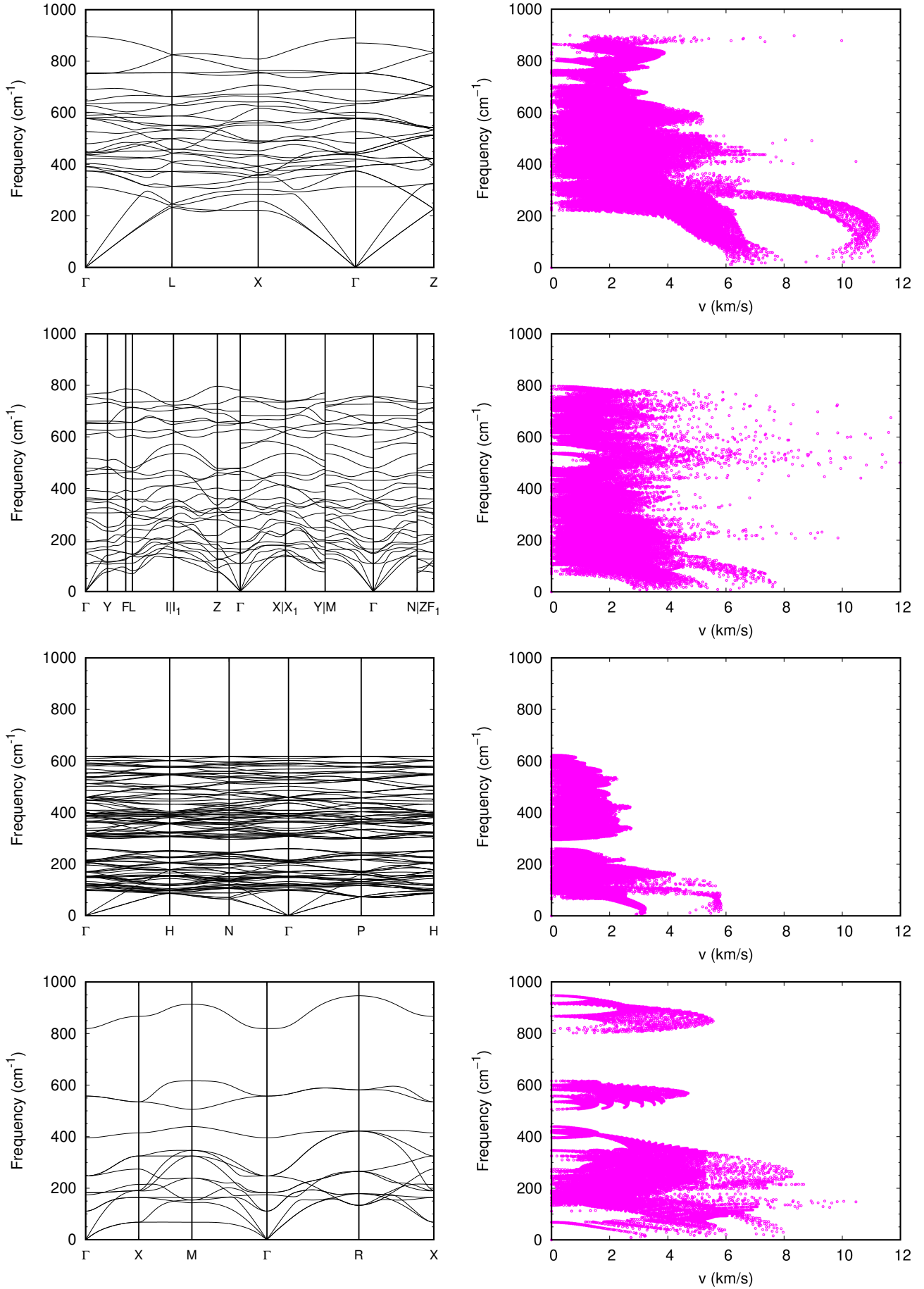


FIG. 3. (Left) Calculated phonon dispersions. (Right) The respective phonon velocities. The compounds are  $\alpha$ -Al<sub>2</sub>O<sub>3</sub>,  $\beta$ -Ga<sub>2</sub>O<sub>3</sub>,  $\beta$ -In<sub>2</sub>O<sub>3</sub> and KTaO<sub>3</sub> from top to bottom, respectively.

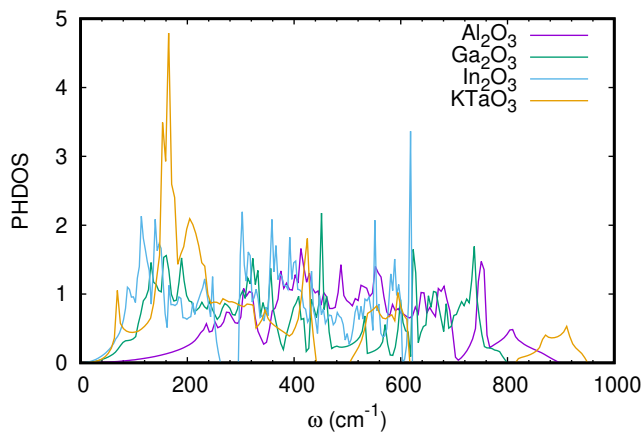


FIG. 4. Calculated phonon density of states normalized to per formula unit (*i.e.* five atoms).

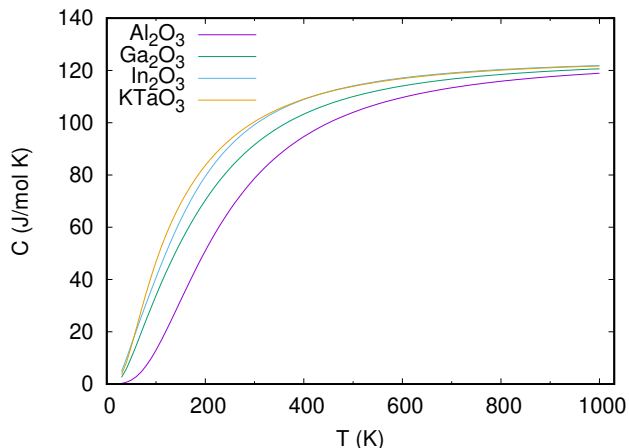


FIG. 5. Calculated molar heat capacity as a function of temperature.

The Grüneisen parameters, which reflect the anharmonicity of phonons, of the four compounds are shown Fig. 6. There is a big overlap of the calculated values throughout the frequency range of the phonon spectrum.  $\alpha$ - $\text{Al}_2\text{O}_3$ 's Grüneisen parameters are positive, reflecting the fact that its phonons harden upon volume contraction.  $\beta$ - $\text{Ga}_2\text{O}_3$  and  $\beta$ - $\text{In}_2\text{O}_3$  additionally have low frequency phonons with negative Grüneisen parameters. The magnitude of the Grüneisen parameters of all three binary compounds are relatively modest and similar, indicating that the variance in the calculated thermal conductivity of these compounds does not primarily derive from the anharmonicity of phonons. However, the Grüneisen parameters of  $\text{KTaO}_3$  are much larger at low frequencies, which implies the presence of stronger three-phonon interactions. This may be the reason why the thermal conductivity of this compound increases more slowly as the temperature is decreased compared to the

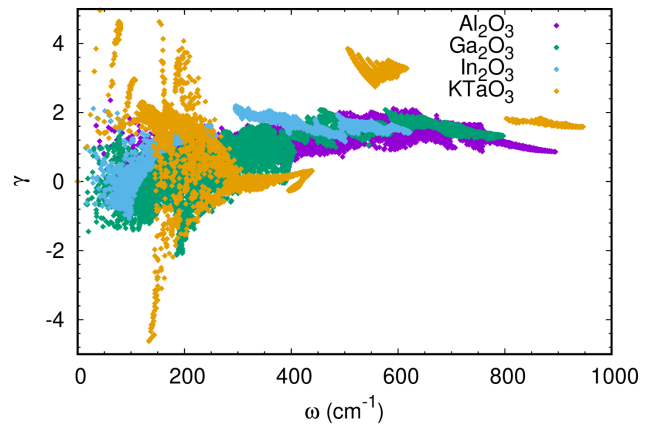


FIG. 6. Calculated Grüneisen parameter for each phonon mode.

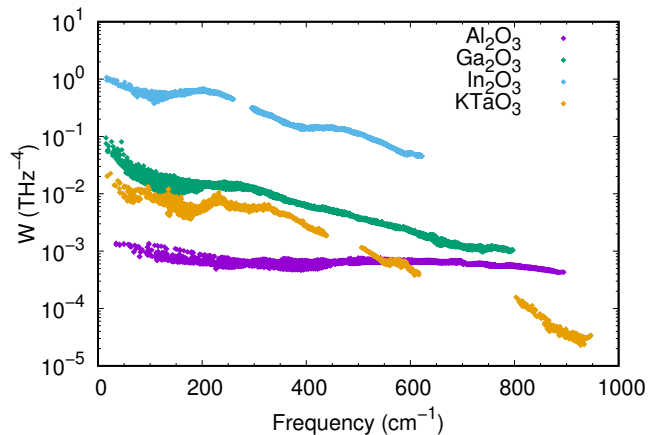


FIG. 7. Calculated weighted three-phonon scattering phase space at 300 K.

three binary compounds.

The calculated weighted scattering phase space available for three-phonon absorption and emission processes of the four compounds is shown in Fig. 7, and they are distinct for each compound. For the three binary compounds, the clear difference in their thermal conductivity is apparent in the scattering phase space. The scattering phase space increases by more than an order of magnitude below  $300 \text{ cm}^{-1}$  each time the cation species moves to the lower row in the periodic table, which unambiguously demonstrates that the scattering phase space is inversely proportional to the calculated thermal conductivity in the three binary compounds. However, the scattering phase space of the ternary compound  $\text{KTaO}_3$  does not follow the same trend. Its scattering phase space at high frequencies is lower by more than an order of magnitude than that of  $\alpha$ - $\text{Al}_2\text{O}_3$ . But at low frequencies, its scattering phase space is larger by an order of magnitude. This suggests that simply have extra elements in

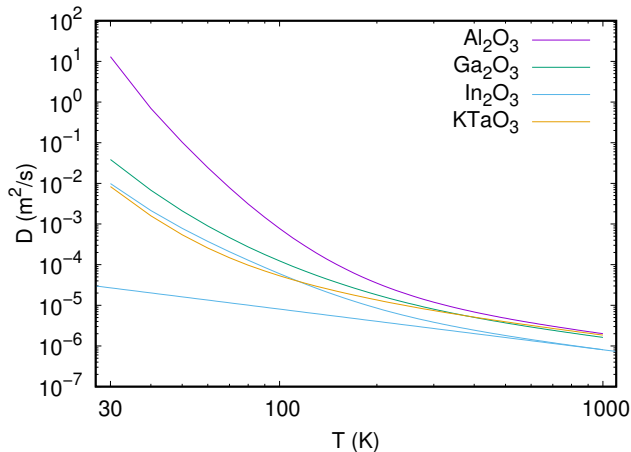


FIG. 8. Calculated thermal diffusivity as a function of temperature. The straight line is calculated using  $v_s = 5.83$  km/s and  $s = 3.11$  obtained for  $\beta$ - $\text{In}_2\text{O}_3$  at 1000 K, and it shows that the calculated diffusivity exhibits a  $T^{-1}$  behavior at high temperatures.

TABLE III. The maximum sound velocity  $v_s$  (km/s) and calculated thermal diffusivities  $D^{\text{th}}$  ( $10^{-6}$  m<sup>2</sup>/s) at 300 and 1000 K of the four materials studied in this work. The experimental diffusivity at room temperature is also given.

	$v_s$	300 K		1000 K
		$D^{\text{th}}$	$D^{\text{exp}}$	$D^{\text{th}}$
$\alpha$ - $\text{Al}_2\text{O}_3$	11.08	11.94	13	2.01
$\beta$ - $\text{Ga}_2\text{O}_3$	7.69	8.04	—	1.63
$\beta$ - $\text{In}_2\text{O}_3$	5.83	3.8	7	0.81
$\text{KTaO}_3$	7.62	7.43	—	1.85

a compound can dramatically increase the three-phonon scattering phase space at low frequencies.

Finally, Fig. 8 shows the thermal diffusivity  $D = \frac{\kappa}{C'}$  of all four compounds calculated using the same data used in Figs. 2 and 5. Here,  $C'$  is the heat capacity per unit volume. The diffusivity approaches a behavior that is proportional to  $T^{-1}$  in all four compounds at high temperatures, which is expected since the heat capacity saturates to a constant value according the Dulong-Petit law and the phonon-phonon scattering rate is proportional to  $T^{-1}$  above the Debye temperature. Although the high-temperature diffusivity has the same temperature dependence in all four compounds, there is some variance in the magnitude of their diffusivity. Again, a look back at the velocity distribution plot in Fig. 3 shows that larger phonon velocities at high frequencies lead to larger high-temperature diffusivity, with  $\beta$ - $\text{In}_2\text{O}_3$  having both low velocities and low diffusivity than the other three materials. The values of high-temperature diffusivity of  $\alpha$ - $\text{Al}_2\text{O}_3$ ,  $\beta$ - $\text{Ga}_2\text{O}_3$ , and  $\text{KTaO}_3$  lie close, and the remaining differences in their relative values of  $D$  in the high- $T$  regime seems to reflect the differences

in their acoustic phonon velocities, as both the acoustic phonon velocities and high- $T$  diffusivity decrease in magnitude going from  $\alpha$ - $\text{Al}_2\text{O}_3$  to  $\text{KTaO}_3$  to  $\beta$ - $\text{Ga}_2\text{O}_3$ .

It has recently been pointed out empirically that there is a lower limit to thermal diffusivity in insulating crystals [28, 29]. The high-temperature diffusivity can be approximately expressed as  $D = sv_s^2\tau_p$ , where  $\tau_p = \frac{\hbar}{k_B T}$  is the Planckian time,  $v_s$  is the sound velocity, and  $s$  is the dimensionless parameter representing the ratio of the average phonon scattering time  $\tau$  to  $\tau_p$ . Experimental data on numerous insulators find a lower-bound  $s > 1$  [29, 30], which implies that phonon-phonon collisions cannot happen faster than the Planckian time. Using the calculated  $v_s$  and  $D^{\text{th}}$  at 300 K, I obtain for  $s$  the values of 3.8 ( $\alpha$ - $\text{Al}_2\text{O}_3$ ), 5.3 ( $\beta$ - $\text{Ga}_2\text{O}_3$ ), 4.4 ( $\beta$ - $\text{In}_2\text{O}_3$ ), and 5.0 ( $\text{KTaO}_3$ ). For comparison, the experiments on  $\beta$ - $\text{In}_2\text{O}_3$  gives  $s = 5.8$  at 300 K [17].

## SUMMARY AND CONCLUSIONS

In summary, I have used first principles calculations to perform a comparative study of thermal conductivity in  $\alpha$ - $\text{Al}_2\text{O}_3$ ,  $\beta$ - $\text{Ga}_2\text{O}_3$ ,  $\beta$ - $\text{In}_2\text{O}_3$  and  $\text{KTaO}_3$ , which was motivated by a recent experimental observation of very high low-temperature  $\kappa$  in  $\beta$ - $\text{In}_2\text{O}_3$  by Xu *et al.* My results on  $\beta$ - $\text{In}_2\text{O}_3$  agrees well with the experimental study, indicating that the peak conductivity value of around 1000 W/mK at low temperatures is an intrinsic property of this material. The calculated  $\kappa$  of  $\beta$ - $\text{Ga}_2\text{O}_3$  is also in reasonable agreement with the available experimental data above 80 K. Additionally, I find that the calculated  $\kappa$  of  $\beta$ - $\text{Ga}_2\text{O}_3$  is larger than that of  $\beta$ - $\text{In}_2\text{O}_3$  at all temperatures, which indicates that  $\beta$ - $\text{Ga}_2\text{O}_3$  can also exhibit peak  $\kappa$  in excess of 1000 W/mK at low temperatures.

I also calculated the thermal conductivity of  $\text{KTaO}_3$  ignoring the temperature-dependent softening of low-frequency phonons to investigate how the microscopic mechanisms for heat transport varies between binary and ternary oxides. At high temperatures, I find that the  $\kappa$  of  $\text{KTaO}_3$  and  $\beta$ - $\text{Ga}_2\text{O}_3$  are similar, reflecting the comparable magnitudes of their acoustic phonon velocities. However, the  $\kappa$  of  $\text{KTaO}_3$  increases less steeply at low temperatures compared to the binary oxides, and  $\text{KTaO}_3$  has the lowest calculated  $\kappa$  despite having acoustic phonon velocities larger than that of  $\beta$ - $\text{In}_2\text{O}_3$ . I attribute this to the fact that the distribution of the velocities of low-frequency acoustic phonons is more scattered in  $\text{KTaO}_3$ , and this results in enhanced momentum loss even during normal phonon-phonon scattering processes. In the binary compounds, the acoustic phonon branches are relatively less dispersive than in  $\text{KTaO}_3$ . This results in a relatively narrower distribution of the acoustic phonon velocities at low frequencies in the binary oxides, which implies that there is less momentum loss when the heat-carrying long-wavelength acoustic phonons scatter

with each other. I think that the differences in acoustic phonon velocity distribution explains why the binary oxides have larger low-temperature  $\kappa$  than the ternary oxides.

Finally, I also calculated the thermal diffusivity using the theoretically obtained thermal conductivity and heat capacity. I find that all four compounds exhibit the expected  $T^{-1}$  behavior at high temperatures. I also used the calculated acoustic phonon velocities to compute the ratio  $s$  of the average phonon scattering time to Planckian time. I find that  $s$  obeys the recently found empirical lower bound of 1 even at 1000 K in all materials, which implies that the phonon-phonon collisions cannot happen faster than the Planckian time.

### ACKNOWLEDGEMENT

I am grateful to Kamran Behnia for discussions and suggestions that motivated this work and for sharing experimental data. The computational resources for this work was provided by GENCi-CINES (grant 2019-A0070911099), the Swiss National Supercomputing Center (grant s820), and the European Research Council (grant ERC-319286 QMAC).

- 
- [1] K. Ellmer, Nat. Photonics **6**, 809 (2012).  
 [2] O. Bierwagen, Semicond. Sci. Technol. **30**, 024001 (2015).  
 [3] G. A. Slack, Phys. Rev. **126**, 427 (1962).  
 [4] D. G. Cahill and R. O. Pohl, Ann. Rev. Phys. Chem. **39**, 93 (1988).  
 [5] B. Dongre, J. Carrete, N. Mingo, and G. K. H. Madsen, MRS Commun. **8**, 1119 (2018).  
 [6] Z. Galazka, K. Irmscher, R. Uecker, R. Bertram, M. Pietsch, A. Kwasniewski, M. Naumann, T. Schulz, R. Schewski, D. Klimm, and M. Bickermann, J. Cryst. Growth **404**, 184 (2014).  
 [7] Z. Guo, A. Verma, X. Wu, F. Sun, A. Hickman, T. Masui, A. Kuramata, M. Higashiwaki, D. Jena, and T. Luo, Appl. Phys. Lett. **106**, 111909 (2015).  
 [8] Z. G. M. Handweg, R. Mitdank, and S. Fischer, Semicond. Sci. Technol. **30**, 024006 (2015).  
 [9] P. Jiang, X. Qian, X. Li, and R. Yang, Appl. Phys. Lett. **113**, 232105 (2018).  
 [10] E. G. Vllora, K. Shimamura, T. Ujiie, and K. Aoki, Appl. Phys. Lett. **92**, 202118 (2008).  
 [11] M. D. Santia, N. Tandon, and J. D. Albrecht, Appl. Phys. Lett. **107**, 041907 (2015).  
 [12] Z. Yan and S. Kumar, Phys. Chem. Chem. Phys. **18**, 29236 (2018).  
 [13] S. Mu, H. Peelaers, and C. G. Van de Walle, Appl. Phys. Lett. **115**, 242103 (2019).  
 [14] R. K. Kremer, K. Graf, M. Cardona, G. G. Devyatikh, A. V. Gusev, A. M. Gibin, A. V. Inyushkin, A. N. Taldenkov, H.-J. Pohl, Solid State Commun. **131**, 499 (2004).  
 [15] Z. Galazka, R. Uecker, K. Irmscher, D. Schulz, D. Klimm, M. Albrecht, M. Pietsch, S. Ganschow, A. Kwasniewski, and R. Fornari, J. Cryst. Growth **362**, 349 (2011).  
 [16] Z. Galazka, R. Uecker, and R. Fornari, J. Cryst. Growth **388**, 61 (2014).  
 [17] L. Xu, B. Fauqué, Z. Zhu, Z. Galazka, K. Irmscher, and K. Behnia, arXiv:2008.13519 [cond-mat.mtrl-sci] (2020).  
 [18] D. G. Onn, A. Witek, Y. Z. Qiu, T. R. Anthony, and W. F. Banholzer, Phys. Rev. Lett. **68**, 2806 (1992).  
 [19] W. Li, J. Carrete, N. A. Katcho, and N. Mingo, Comput. Phys. **185**, 1747 (2014).  
 [20] W. Li and N. Mingo, Phys. Rev. B **89**, 184304 (2014).  
 [21] J. Fabian and P. B. Allen, Phys. Rev. Lett. **79**, 1885 (1997).  
 [22] G. Kresse and J. Furthmüller, Phys. Rev. B **54**, 11169 (1996).  
 [23] H. Peelaers and C. G. V. de Walle, Phys. Status Solidi B **252**, 828 (2015).  
 [24] A. Togo and I. Tanaka, Scr. Mater. **108**, 1 (2015).  
 [25] Y. Fu and D. J. Singh, Phys. Rev. Materials **2**, 094408 (2018).  
 [26] G. A. Slack, J. Phys. Chem. Solids **34**, 321 (1973).  
 [27] G. A. Slack, Solid State Phys. **34**, 1 (1979).  
 [28] V. Martelli, J. L. Jiménez, M. Continentino, E. Baggio-Saitovitch, and K. Behnia, Phys. Rev. Lett. **120**, 125901 (2018).  
 [29] K. Behnia and A. Kapitulnik, J. Phys.: Condens. Matter **31**, 405702 (2019).  
 [30] C. H. Mousatov and S. A. Hartnoll, Nature Physics **16**, 579 (2020).